# **Weight function calculation method for analyzing mixed-mode shear cracks in reinforced concrete beams**

Pengru Deng[1*] and Takashi Matsumoto[2]

[1]Assistant professor, Faculty of Engineering, Hokkaido University, Hokkaido 060-8628, Japan; Tel: +81-11-706-6172; Email: pengrudeng@eng.kokudai.ac.jp

[2]Professor, Faculty of Engineering, Hokkaido University, Hokkaido 060-8628, Japan; Tel: +81-11-706-6171; Email: takashim@eng.kokudai.ac.jp

*Corresponding author

## ABSTRACT

Based on a virtual crack extension (VCE) technique in finite element method (FEM), this paper proposes a rational method of calculating weight functions for inclined shear cracked RC beams with any geometry. As an inclined shear crack in an RC beam is geometrically determined by the absolute dimensions, shear span to beam depth ratio, crack inclined angle and crack initiation location, the relations between the weight functions and these parameters are investigated by either following theoretical equations or varying the parameters in a certain range. The range is determined to enclose the geometries of inclined critical shear cracks of a large set of RC beams which were tested under a bending load but failed due to the propagation of a critical inclined shear crack. Moreover, a method of calculating the weight functions of a shear cracked RC beam with any geometrical properties is developed numerically using the weight functions calculated and provided in this study. As a result, it is possible that the shear behaviors of RC beams can be even studied conveniently but also comprehensively following the theoretical fracture mechanic approach.

**KEYWORDS**: Shear crack; Reinforced concrete beam; Fracture mechanics; Weight function; FEM.

**Nomenclature**

| | |
|---|---|
| $a$ | crack length |
| $\beta$ | crack inclined angle |
| $\beta^r$ | crack inclined angle of the reference case |
| $\beta^a$ | crack inclined angle of an arbitrary case |
| $c$ | depth of the compression zone |
| $C_f$ | resultant normal force of concrete in the compression zone |
| $\Delta a$ | the amount of virtual crack extension |
| $\delta$ | the maximum deflection |
| $E$ | Young's modulus |
| $f_c$ | strength of concrete |
| $\{f_{I(II)}\}$ | decomposed nodal force vectors |
| $\varphi$ | crack initiation location ratio |
| $\varphi^r$ | crack initiation location ratio of the reference case |
| $\varphi^a$ | crack initiation location ratio of an arbitrary case |
| $\gamma_1$ | depth ratio of the equivalent rectangular stress block |
| $H$ | effective modulus |
| $h$ | width of the shear span |
| $h_1$ | crack initiation location |
| $h_{I(II)}$ | mode I and II weight function components |
| $I$ | sectional moment of inertia of the beam |
| $[J]$ | Jacobian matrix between local coordinates and global coordinates |
| $[K]$ | global stiffness matrices |
| $[k_i]$ | elemental stiffness |
| $K_{I(II)}$ | mode I and II stress intensity factors |
| $l_s$ | size of the first ring of elements around the crack tip |
| $\mu$ | displacement constant depending on boundary conditions and applied load |
| $N_c$ | number of elements around the crack tip |
| $v$ | Poisson's ratio |
| $\omega$ | shear span/beam depth ratio |
| $\omega^r$ | shear span/beam depth ratio of the reference case |
| $\omega^a$ | shear span/beam depth ratio of an arbitrary case |
| $P$ | applied reference load |
| $\rho$ | longitudinal steel ratio |
| $\sigma_{xx}$ | normal stress in the local $x$ direction |
| $\sigma_{yy}$ | normal stress in the local $y$ direction |
| $\sigma_{xy}$ | shear stress in the local $x$-$y$ plane |
| $U_{I(II)}$ | decoupled nodal displacement |
| $w$ | effective depth of reinforcement |
| $w^a$ | effective depth of reinforcement of an arbitrary case |

## 1 INTRODUCTION

It is generally believed that a well-designed reinforced concrete (RC) beam subjected to extreme overloads should fail in a ductile and symptomatic flexure mode rather than a brittle and catastrophic shear mode [1]. However, as the shear behaviors of RC beams have not been fully uncovered, the shear failure appeared as one of the commonly observed failure modes of RC beams under service. As a result, the related design codes are continually changing and normally becoming more stringent [2, 3]. Referencing to current codes, even structures that were designed in the last few decades may not satisfy the requirements of the latest codes, which implicates that massive amount of funds may have to be spent on rehabilitating or upgrading the infrastructures. Therefore, it is of great significance to develop a comprehensive model, free of empirical limitations, for analyzing the shear behaviors and strength of RC beams.

For a shear critical RC beam, it was concluded that the shear behaviors and strength are associated with the opening of a major inclined shear crack and a breakdown along this crack. Focusing on this critical inclined shear crack, researchers believe that it is difficult to predict the post-diagonal cracking behaviors reliably. As a result, the ultimate failure load was roughly assumed to be equivalent to the inclined cracking load. However, it was observed that some tested RC beams failed at loads 100% greater than the inclined cracking loads [4], which means attentions should be paid to the post-cracking behaviors including the propagation of the inclined critical shear crack. In terms of the post-cracking behaviors, it was confirmed that an aggregate interlock in transferring shear stresses across the diagonal shear crack plays a key role [5, 6]. Fenwich and Paulay also reported that it is the breakdown of aggregate interlock action that triggers the shear failure based on detailed measurements of a group of cracked beams [7]. In addition, Walraven's studies showed that this shear stress transmitted by aggregates is related to the crack width [8]. Similarly, the shear resistance from the longitudinal reinforcement was reported to have been underestimated by empirically derived ACI expression [2]. All the findings improved the cognition of the shear failure mode of RC beams but complicated or even encumbered the development of a comprehensive analytical model.

Fortunately, a weight function (WF) concept in fracture mechanics [9, 10] provides a possibility for the development of a comprehensive analytical model. Attributing to the load-independent characteristic of WFs, the crack tip stress intensity factors (SIFs) as well as the cracking opening displacements (CODs) under any loading conditions can be calculated with the WFs for the cracked geometry if the crack face stresses from bridging elements, such as aggregates and rebar are related to the crack width. As the nonlinearities such as the fictitious cracks in the fracture processing zone (FPZ) can be included in the bridging stress to crack width relations [11], the WF which is a concept in the linear elastic fracture mechanics (LEFM) may be extended to nonlinear fractures. Using the analytical WFs for the Mode I crack [12], both the SIFs and CODs of flexural cracks in RC beams have been calculated in Ref. [13-15]. In fact, the WFs are also applicable for analyzing beams made of other composite materials, e.g., fiber reinforced concrete (FRC) and polymer cement mortar (PCM), as well as beams with externally attached reinforcements, e.g., carbon fiber reinforced polymer (CFRP) sheet, if the bridging effect can be equivalent to stresses relating the cracking width [16-19]. Inversely, the stresses of the bridging elements can be predicted exploiting the COD profiles measured in real structures as implemented in [13-15]. Similarly, in terms of the inclined shear cracks, it is also feasible to study the cracking behaviors theoretically based on fracture mechanics if the mixed mode WFs for the shear cracked beam geometries can be calculated conveniently, even if not the closed-form analytical expressions like the Mode I crack. However, no such a method of calculating WFs is available for the shear cracked beam so far.

Therefore, this study aims at proposing a method of calculating WFs for shear cracked RC beams based on a virtual crack extension (VCE) technique in finite element method [20-22]. Actually, exploiting the mixed mode WFs from this method, the authors have successfully predicted the fatigue life and determined the dominant degradation mechanisms of RC slabs under a moving wheel-type load focusing on the propagation and failure along a couple of critical punching shear cracks [23, 24].

As the critical shear crack in beams is normally characterized as an approximately inclined straight-line [25, 26], the shear cracked RC beams may be geometrically determined by the absolute dimensions, shear span/beam depth ratios, crack initiation location and crack inclined angle. Hence, firstly, this study is dedicated to obtained the relations between the WFs and the geometrical parameters by varying each parameter in a certain range. To be efficiency, the ranges are determined beforehand to enclose the crack initiation locations and crack inclined angles of the critical shear crack of a large set of experimental RC beams. With the obtained results and through theoretical analyses, it is found that the WFs along all the boundaries of a shear cracked beam of any geometrical properties can be calculated exploiting the corresponding WFs of only one or two beams with different geometries. Furthermore, a WF calculation method for analyzing the beams with shear cracks is developed to facilitate applications.

## 2 DIAGONAL SHEAR CRACKS IN RC BEAMS

Generally, as shown in **Fig. 1**, the critical shear crack of an RC beam consists of two branches, whereas the crack propagation in the second branch is unstable. Once the crack tip reaches the second branch, a brittle failure is caused by a splitting of concrete and along the second branch line as reported in Ref. [27]. Therefore, this study focuses on the first branch and provides a convenient WF calculation method for further analyses on the cracking behaviors of the critical shear cracks in RC beams based on fracture mechanics.

For a given RC beam, the first branch is geometrically determined by a crack inclined angle ($\beta$) and crack initiation location ($h_1$), which can be calculated following the methods introduced in Ref. [27] and simply reinterpreted as follows. According to ACI code [2], the distance of the normal concrete force $C_f$ from the compression fiber is $0.5\gamma_1 c$ as shown in **Fig. 1**, where $c$ is the depth of compression zone above the tip of the inclined shear crack. This $\gamma_1 c$ which depends on the strength of concrete $f_c$ is the depth of the equivalent rectangular stress block. For simplicity, a mean value of 0.72 is assigned to $\gamma_1$ for all values of concrete $f_c$ in this study. Based on a principle that the sum of moments (about the tip of the inclined crack) of the forces acting on the right part of the beam shown in **Fig. 2** is equal to zero, the inclined angle $\beta$ should satisfy an equation expressed as [27]

$$cot^2\beta - \frac{h/w}{1 - c/w} cot\beta + \frac{2.5 - c/w}{1 - c/w} \tag{1}$$

where $h$ and $w$ are the width of the shear span and the effective depth of reinforcement, respectively; $c$ can be calculated according to **Eq. (2)** if the maximum compression strain of concrete and elastic modulus of reinforcement are assumed as 0.002 and $2\times10^5$MPa, respectively. These values are acceptable for general cases. With these values and following [27], one obtains

$$\left(\frac{c}{w}\right)^2 + 600\frac{\rho}{f_c}\frac{c}{w} - 600\frac{\rho}{f_c} = 0 \tag{2}$$

where $\rho$ is a longitudinal steel ratio which is equal to the cross-sectional area of longitudinal steel rebars dividing the beam cross-sectional area.

In addition, following the geometrical relations as schematically shown in **Fig. 1**, the distance $h_1$ of the initiation of shear crack from the support can be expressed as

$$\frac{h_1}{w} = \left(1 - \frac{c}{w}\right)\left(\frac{h/w}{1 - 0.36\, c/w} - cot\beta\right) \tag{3}$$

Finally, with the compression depth ($c$), crack inclined angle ($\beta$), and crack initiation location ($h_1$) from solving **Eq. (1) - (3)**, the geometrical information for the first branch of the critical inclined shear crack can be obtained.

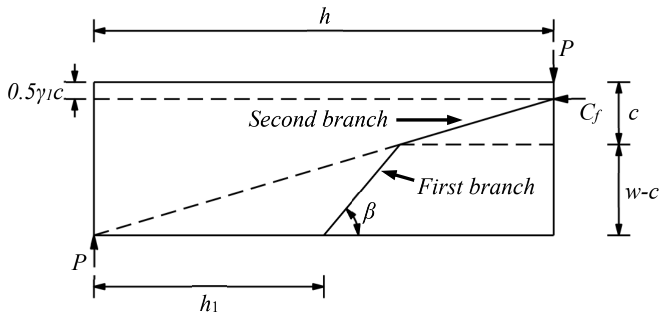


**Fig. 1.** Geometrical representation of critical inclined crack

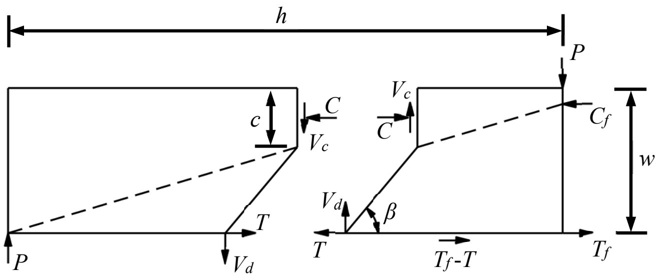


**Fig. 2.** Forces acting on portions of beam where splitting occurs

## 3 FORMULATIONS FOR MIXED FRACTURE MODE

The WFs are, in fact, the Green's function for the SIFs in a cracked body. For 2-D mixed mode cracks, exploiting the VCE technique in FEM combined with symmetric mesh in the crack tip neighborhood as shown in **Fig. 3**, the SIFs and nodal WFs are decoupled into Model I and Mode II components because the symmetric mesh provides the decoupled characteristics for the stresses, strains, displacements and traction field parameters into Mode I and II components with respect to $x$ axis [22]. For a crack length ($a$) and inclination angle ($\beta$), the decoupled nodal Mode I WF components $h_{Ix(y)}$ and Mode II WF components $h_{IIx(y)}$ at $i$'s nodal location ($x_i$, $y_i$) can be expressed with the corresponding displacement differentiations ($\partial U_{I(II)}/\partial a$) and SIFs ($K_{I(II)}$) as

$$h_{I(II)x}(x_i, y_i, a, \beta) = \frac{H}{2K_{I(II)}} \frac{\partial U_{I(II)x}(x_i, y_i, a, \beta)}{\partial a} \tag{4}$$

$$h_{I(II)y}(x_i, y_i, a, \beta) = \frac{H}{2K_{I(II)}} \frac{\partial U_{I(II)y}(x_i, y_i, a, \beta)}{\partial a} \tag{5}$$

where $H$ is an effective modulus which is $E$ for plane strain and $E/(1-v^2)$ for plane strain. $E$ and $v$ are material Young's modulus and Poisson's ratio, respectively. Subscript $_{I(II)}$ means Mode I and Mode II components. Thus, $h_{I(II)x}$ and $h_{I(II)y}$ are WF components along the $x$ and $y$ axes in $(x, y)$ coordinate system respectively for Mode I or II fracture problems. Correspondingly, $U_{I(II)x}$ and $U_{I(II)y}$ are the displacement components along the $x$ and $y$ axes respectively for Mode I or II deformation, which can be determined according to [22] within the symmetric region in the crack tip neighborhood. From **Eq. (4)** and **(5)**, it is found that, in order to obtain the nodal WFs, the displacement differentiations ($\partial U_{I(II)}/\partial a$) and SIFs ($K_{I(II)}$) should be expressed with data that can be output from FEM, such as global stiffness matrices and nodal displacement vectors.

For Mode I and Mode II SIFs $K_{I(II)}$, they can be obtained following their relationships with strain energy release rate which is the change in potential energy in a given loading system produced by the virtual crack extension. And $K_{I(II)}$ can be expressed as

$$K_{I(II)} = \left\{ H \left[ -\frac{1}{2} \{U_{I(II)}\}^T \frac{\partial [K]}{\partial a} \{U_{I(II)}\} + \{U_{I(II)}\}^T \frac{\partial \{f_{I(II)}\}}{\partial a} \right] \right\}^{1/2} \tag{6}$$

where $[K]$ and $\{f_{I(II)}\}$ are the global stiffness matrices and decomposed nodal force vectors, respectively. And $\partial[K]/\partial a$ and $\partial\{f_{I(II)}\}/\partial a$ are the changes of $[K]$ and $\{f_{I(II)}\}$ due to the VCE as shown in **Fig. 3**. Obviously, $\partial\{f_{I(II)}\}/\partial a$ equals 0 in the absence of body-force loading, thermal loading, and crack-face loading conditions, which can be ensured for RC beam analyses where the crack-face bridging stresses are considered separately. As $[K]$ is an integration of all elemental stiffness $[k_i]$ which depends on the individual elemental geometry, shape function and elastic properties, the variation of the global stiffness matrices with respect to the VCE $\partial[K]/\partial a$ is given as

$$\frac{\partial[K]}{\partial a}=\sum_{i=1}^{N_c}\frac{[k_i]|_{a+\Delta a}-[k_i]|_a}{\Delta a} \tag{7}$$

where $[k_i]$ is elemental stiffness matrix. $N_c$ is the number of elements around the crack tip because only the elemental geometry of crack tip elements is perturbed by the VCE as shown in **Fig. 3**. $\Delta a$ is the amount of VCE in a direction collinear with the oblique crack.

For the decoupled displacement derivatives, $\partial\{U_{I(II)}(x_i, \mathrm{y_i}, a, \beta)\}/\partial a$, they can be obtained through applying a chain rule of differentiation of $U_{I(II)}(x_i, \mathrm{y_i}, a, \beta)$ with respect to the crack length ($a$). Considering the inclined angle $\beta$ for a given shear crack is constant, the obtain decoupled displacement derivatives are expressed as

$$\frac{\partial\{U_{I(II)}\}}{\partial a}=\frac{d\{U_{I(II)}\}}{da}-\frac{\partial\{U_{I(II)}\}}{\partial x}\cdot\frac{dx}{da}-\frac{\partial\{U_{I(II)}\}}{\partial y}\cdot\frac{dy}{da} \tag{8}$$

Since the stresses, strains, and displacements should satisfy the equilibrium equation and compatibility condition as

$$[K]\{U_{I(II)}\}-\{f_{I(II)}\}=0 \tag{9}$$

Taking total differentiation of **Eq. (9)** with respect to crack length ($a$) and after rearrangement, the first term in the right part of **Eq. (8)** is given as

$$\frac{d\{U_{I(II)}\}}{da}=[K]^{-1}\left[\frac{d\{f_{I(II)}\}}{da}-\frac{d[K]}{da}\{U_{I(II)}\}\right] \tag{10}$$

where $[K]^{-1}$ is the inverted matrix of the global stiffness of original crack geometry. $d\{f_{I(II)}\}/da$=0.0 for the targeted case. As among the three determinants of the global stiffness matrix $[K]$, i.e. elemental geometry, shape function and elastic properties, the elemental geometry is the only factor that relates to the crack length, $d[K]/da$ should be the same as $\partial[K]/\partial a$ and can be calculated following **Eq. (7)**.

The last two terms of **Eq. (8)** serve as the correction factors of changing the total displacement derivatives to partial displacement derivatives for the oblique cracks, which are null for nodes without geometric changes as a result of VCE. For a collinear VCE with an oblique crack, we have $dx/da$=1.0 and $dy/da$=0. The finite element evaluation of $\partial\{U_{I(II)}\}/\partial x$ in **Eq. (8)** resulting from the VCE can be obtained following [22] using a Jacobian matrix [$J$] between local coordinates and global coordinates.

Substituting **Eq. (6)** and **Eq. (8)** into **Eq. (4)** and **Eq. (5)**, the nodal WFs for Mode I and Mode II for an oblique edge crack geometry with crack length ($a$) and inclination angle ($\beta$) at ($x_i$, $y_i$) locations can be obtained and expressed as

$$h_{I(II)x}(x_i, y_i, a, \beta) = \frac{H}{2K_{I(II)}}\left\{\frac{d\{U_{I(II)x}\}}{da} - \frac{\partial\{U_{I(II)x}\}}{\partial x}\frac{dx}{da}\right\} \quad (11)$$

$$h_{I(II)y}(x_i, y_i, a, \beta) = \frac{H}{2K_{I(II)}}\left\{\frac{d\{U_{I(II)y}\}}{da} - \frac{\partial\{U_{I(II)y}\}}{\partial x}\frac{dx}{da}\right\} \quad (12)$$

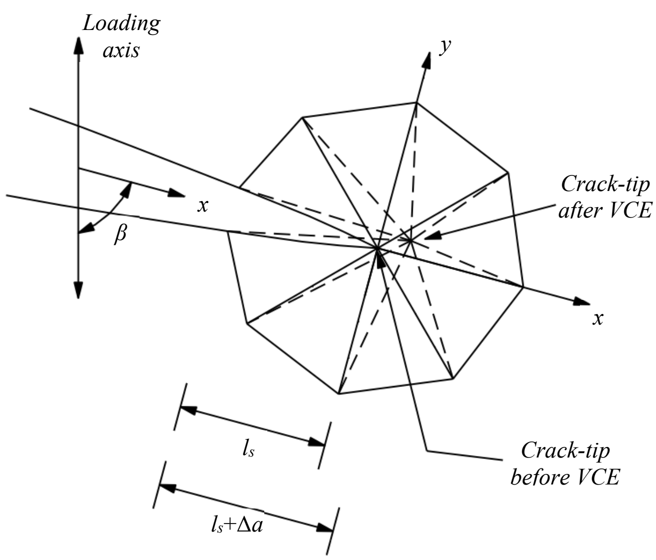


**Fig. 3.** Symmetric mesh in crack tip neighborhood with respect to the global $x$ axis

## 4 RESULTS AND DISCUSSIONS

### 4.1 Shear crack geometry for RC beams

To improve calculation efficiency, the initiation locations and inclined angles are calculated beforehand for the critical shear cracks in sets of RC beams from a series of literatures. And then, the WF variations with respect to these two parameters will be investigated in two ranges which can enclose the geometries of the employed RC beams. Applying the introduced theories in **section 2**, the theoretical crack initiation locations and inclined angles are evaluated and shown in **Fig. 4** for the sets of RC beams tested by [5, 29-36]. As the exploited beams are with various strengths of concrete (from 10.5 MPa to 98.8 MPa), reinforcement ratios (from 0.5% to 3.36%), shear span to beam depth ratios, and absolute geometrical sizes (beam depth ranging from 7 cm to 120 cm), they are of good representative of the RC beams failed due to a critical shear crack. From **Fig. 4**, it is found that the crack initiation location ($h_1/h$) and inclined angle ($\beta$) for almost all the RC beams fall in two ranges of {0.4, 0.6} and {40°, 60°}, respectively. Thus, to be efficient, these two ranges are employed for further calculations of obtaining the relations between the WFs and the two geometrical properties in this study.

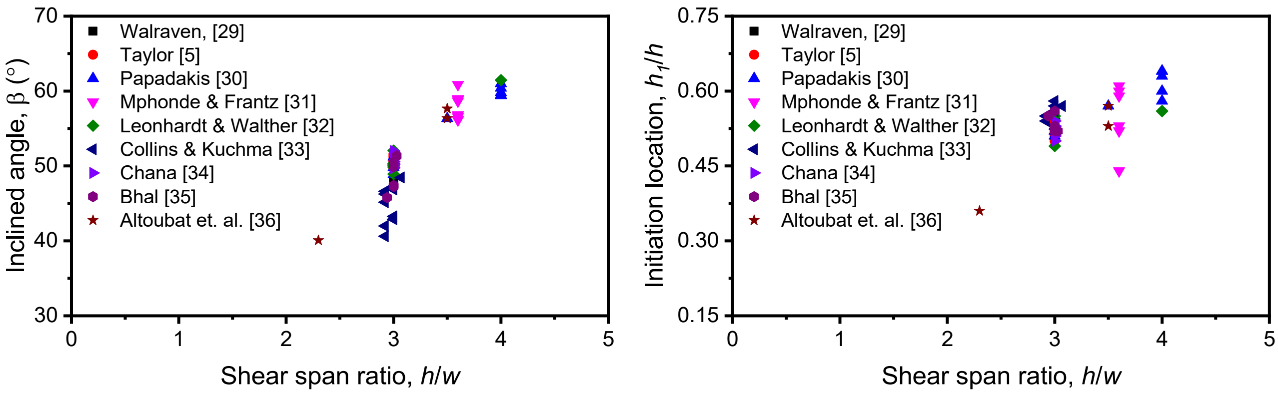


($a$) Inclined angle vs. shear span ratio ($b$) Initiation location vs. shear span ratio

**Fig. 4.** Initiation locations and inclined angles for critical shear cracks in RC beams

### 4.2 Weight function

This study aims at uncovering and summarizing the relations between all WFs along the general load applied boundaries and all the parameters which geometrically determine a shear cracked RC beam (**Fig. 5**), i.e. absolute dimensions, shear span/beam depth ratios ($h/w$), crack initiation location ($h_1/h$) and crack inclined angle ($\beta$). In this study, the shear span/beam depth ratio and the crack initiation location are simply represented by $\omega$ and $\varphi$, respectively. In this study, focuses will be concentrated on investigating and deducing the variations and regulations of WFs with respect to these geometrical parameters.

As the dependence of WF on constraint conditions for a given crack geometry can be circumvented as reported in Ref. [16], a simple constraint condition shown in **Fig. 6** is employed for all calculations. A pure bending load condition as shown in **Fig. 6** is employed considering the load-independent of WFs. To capture the $1/\sqrt{r}$ singular behavior of crack face WFs in the crack tip neighborhood, the triangular quarter-point elements are employed for the first ring of elements around the crack tip [28]. The size of the first ring of elements is set as $l_s/a$=0.04, which can ensure a high enough accuracy. As generally possessed for VCE technique, the amount of crack extension ($\Delta a$) is one of the key operational parameters. A $10^{-5}$ was determined as an appropriate value crack extension ratio ($\Delta a/l_s$) for evaluating both Mode I and Mode II WFs accurately.

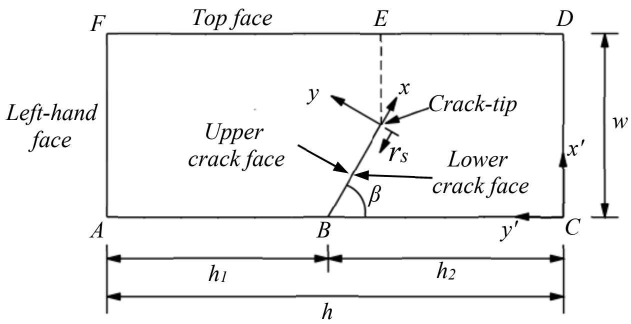


**Fig. 5.** Geometry for the inclined shear crack

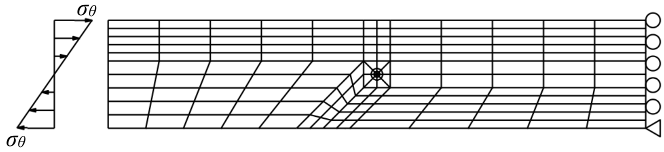


**Fig. 6.** Finite element model of the cracked beam under pure bending load

### 4.2.1 Weight function for varying absolute dimensions

For a unit width beam as shown in **Fig. 5** under any boundary conditions and a given reference load, the maximum deflection of the beam ($\delta$) can be calculated

$$\delta = \mu \cdot \frac{Ph^3}{EI_1} \tag{13}$$

where $P$ is the applied reference load. $\mu$ is a constant which is dependent on the boundary conditions and the location of the applied load. $h$ is the span of the beam. $E$ and $I$ are the Young's modulus and the sectional moment of inertia of the beam, respectively. For a unit width of beam, $I$ is given as

$$I_1 = \frac{1 \cdot w^3}{12} \tag{14}$$

where $w$ is the depth of the beam as shown in **Fig. 5**.

In terms of a given elastic beam under an unchanged reference load, if all the absolute values of the geometrical dimensions including $h$, $w$ as well as the virtual crack extension ($\Delta a$) are increased to n times, it is found that the maximum deflection ($\delta$) of the beam will stay unchanged by substituting **Eq. (14)** into **Eq. (13)**. Thus, for an elastic body, the displacement distributions should stay unchanged as well. Nevertheless, as the value of the geometrical crack extension ($\Delta a$) is increased to *n* times, the partial derivation of displacement distributions with respect to the virtual crack extension, the terms $\partial\{U_{I(II)}\}_x/\partial a$ and $\partial\{U_{I(II)}\}_y/\partial a$ in **Eq. (4) - (5)**, should be reduced to $1/n$. Besides, for the plane stress and strain conditions, the global stiffness matrix is dimensional independent. Substituting these terms after changing the absolute dimensions into **Eq. (4) - (6)**, it is found that both SIF and WF components under an unchanged reference load should be reduced to $1/\sqrt{n}$ with respect to the n times of dimension increase. Therefore, the WFs for any shear cracked RC beams can be easily calculated exploiting the corresponding WFs of one shear cracked RC beam with the same geometries with different absolute dimensions.

### 4.2.2 Weight function for varying inclination angle

In order to investigate the relation between the crack inclination angle and WFs, other geometrical parameters should stay unchanged. In this section, for the oblique cracked geometry shown in **Fig. 5**, $h$=300mm, $w$=100mm, $a/w$=0.5 and $\varphi$ =0.6 are employed for calculation. And, the inclined edge cracked geometries with an inclined angle in the identified range, i.e. from $\beta$=40° to $\beta$=60°, are employed for the detailed WF calculation. With respect to the ($x'$, $y'$) coordinates and $\beta$ from 40° to 60°, **Fig. 7** shows the nodal WF components along the left-hand face of the inclined edge cracked geometries in relation to the distance from the point $A$ (**Fig. 5**). For a given inclined angle $\beta$, it is found that $h_{Ix'}$ and $h_{IIx'}$ stay almost constant while $h_{Iy'}$ and $h_{IIy'}$ decrease linearly to even below zero in a certain range adjacent to point $F$ once the concerned point passes the altitude of the crack tip in the vertical upward direction. In terms of the WFs for different inclined angle, it is found that the absolute values of $h_{Ix'}$ and $h_{IIx'}$ decrease almost linearly with respect to the increasing inclined angle as shown in **Fig. 8**. In terms of $h_{Iy'}$ and $h_{IIy'}$, as these two WF components exhibit an approximately linear correlation with respect to the distance away from point $A$ as observed in **Fig. 7**, it might be fitted well employing a function as

$$f(t) = k_1 t + k_2 \tag{15}$$

where $t$ is the distance away from point $A$. $k_1$ and $k_2$ are the slope and vertical intercept of the fitted equations, respectively. For all the selected inclined angles, both $k_1$ and $k_2$ for $h_{Iy'}$ and $h_{IIy'}$ are shown as black continuous curves in **Fig. 9** and **10**, respectively. After these fittings, one couple of $k_1$ and $k_2$ can represent the distribution one WF component along the left-hand face, which means that a deriving of the variations of $h_{Iy'}$ and $h_{IIy'}$ with changing inclined angle is transformed into a deriving of the relations between $k_1$ and $k_2$ and the inclined angle. Besides, as an approximate linear relation is observed between the two fitting coefficients, i.e. $k_1$ and $k_2$, and the inclined angle (see. **Fig. 7**), if they are available for two different inclined angles, the values of $k_1$ and $k_2$ of any other inclined angles among or outside of the range enclosed by the two angles may be obtainable employing either linear interpolation or extrapolation, respectively. Using $k_1$ and $k_2$ for 40° and 60° and conducting linear interpolation, the $k_1$ and $k_2$ for the other inclined angles are calculated as shown with isolated triangle points in **Fig. 9** and **10**, where a very high accuracy is achieved in all cases. Therefore, it may be concluded that for any inclined angles, both $h_{Ix'}$, $h_{IIx'}$ and $h_{Iy'}$, $h_{IIy'}$ along the left-hand face can be determined using the corresponding results from two inclined angles.

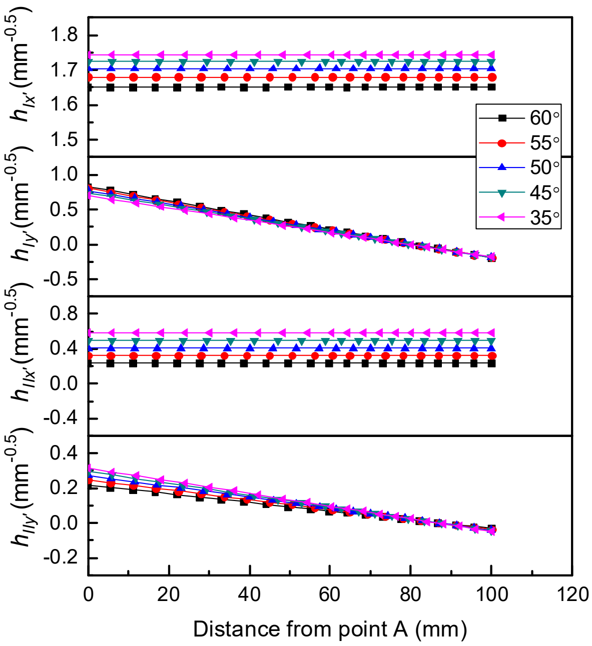


**Fig. 7.** Weight function variations with changing crack inclined angle for left-hand face

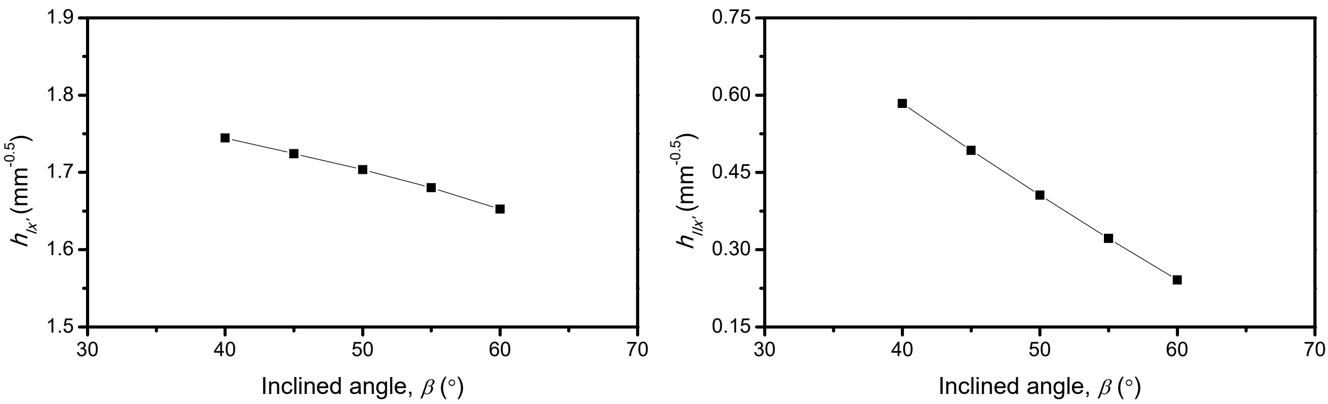


($a$) $h_{Ix'}$ ($b$) $h_{IIx'}$

**Fig. 8.** Constant values of $h_{Ix'}$ and $h_{IIx'}$ with respect to distance from point A on left-hand face for different crack inclined angles

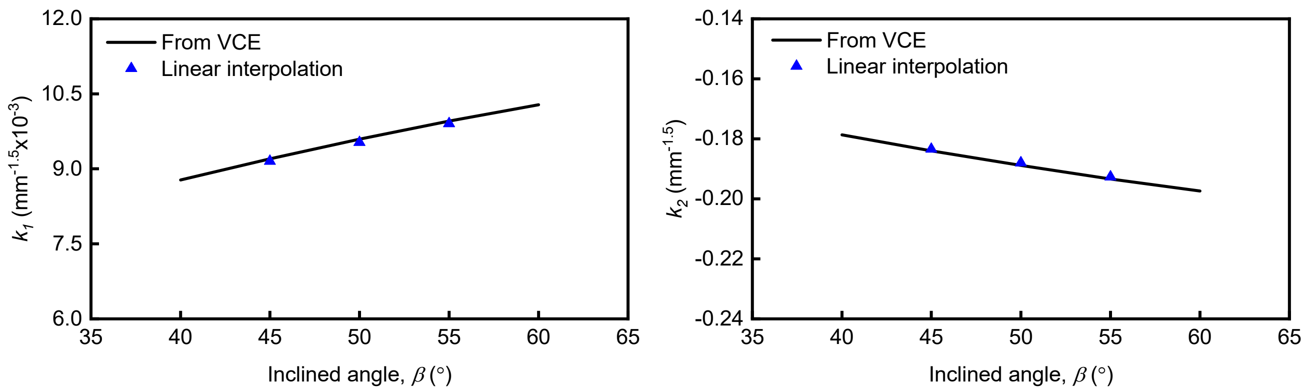


(a) Linear interpolation of $k_1$ (b) Linear interpolation of $k_2$

**Fig. 9.** Linear interpolation of $k_1$ and $k_2$ for $h_{Iy'}$ along left-hand face for different inclined angles

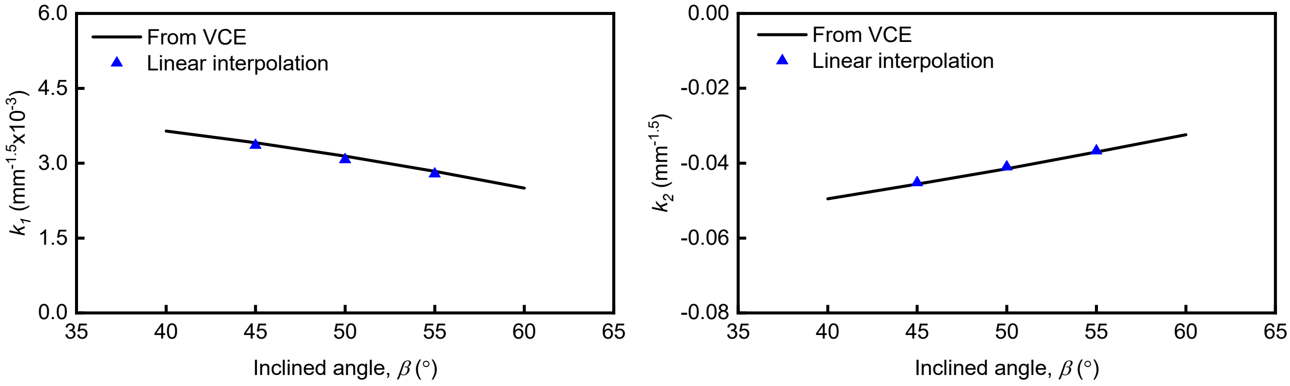


(a) Linear interpolation of $k_1$ (b) Linear interpolation of $k_2$

**Fig. 10.** Linear interpolation of $k_1$ and $k_2$ for $h_{IIy'}$ along left-hand face for different inclined angles

Theoretically, all the orderly trends exhibited in the curves can be understood as follows. As shown in **Fig. 11**, for a 2-D crack geometry subjected to any arbitrary loading condition combining both Mode I and Mode II fracture components, the stress state of any point around the crack tip can be related to Mode I and Mode II SIFs by a matrix of constants which can be simply expressed as

$$\begin{Bmatrix} \sigma_{xx} \\ \sigma_{yy} \\ \sigma_{xy} \end{Bmatrix} = \frac{1}{\sqrt{2\pi r}} \begin{bmatrix} cos(\theta/2)[1 - sin(\theta/2)sin(3\theta/2)] & -sin(\theta/2)[2 + cos(\theta/2)cos(3\theta/2)] \\ cos(\theta/2)[1 + sin(\theta/2)sin(3\theta/2)] & sin(\theta/2)cos(\theta/2)cos(3\theta/2) \\ sin(\theta/2)cos(\theta/2)cos(3\theta/2) & cos(\theta/2)[1 - sin(\theta/2)sin(3\theta/2)] \end{bmatrix} \cdot \begin{Bmatrix} K_I \\ K_{II} \end{Bmatrix} \quad (16)$$

where $r$ and $\theta$ are the coordinates of the concerned location as shown in **Fig. 11**. For a given location, the second term on the right part of **Eq. (16)** should be a matrix of constants. According to the WF concept, the WFs at a point on a cracked geometry are equivalent to the SIFs in values if a unit concentrated load is applied at the point. Hence, the $h_{Ix'}$, $h_{IIx'}$ and $h_{Iy'}$, $h_{IIy'}$ at a point on the left-hand face can be obtained if a unit load is applied at the point along the $x'$ and $y'$ axes, respectively. In the scale of elastic mechanics, it is easily imaginable that the stresses of any point around the crack-tip may stay constant if a unit applied load along the $x'$ axis moves from point $A$ to $F$ (see. **Fig. 5**) owing to the unchanged force lever with respect to the crack tip.

Similarly, the stresses of any point around the crack-tip should decrease linearly if a unit applied load along the $y'$ axis moves from point $A$ to $F$. These trends should be and are exhibited in the corresponding WF curves as shown in **Fig. 7**. And, due to a decrease of force lever with an anti-clockwise rotation of crack face as shown in **Fig. 8**, the absolute values of $h_{Ix'}$ and $h_{IIx'}$ decrease with an increasing of the inclined angle. The reason why negative values are observed in $h_{Iy'}$ and $h_{IIy'}$ can be explained as follows. For a point load applied on the left-hand face along $y'$ axis, it has two effects on the crack beam cross section. One is tension which leads to crack opening and the upper crack face sliding along the positive direction of $x'$. Another one is rotation which has the same effects as those of tension when the point load is below the crack tip. If the point load passes the crack tip, the effects of the rotation turn to the opposite direction, i.e. crack closing and the upper face sliding along the negative direction of $x'$. As the opposite effects of rotation increase as the loading point approaches to the point $F$, they may surpass the effects of tension and, consequently, negative values are observed in $h_{Iy'}$ and $h_{IIy'}$ in certain ranges adjacent to point $F$. This theoretical interpretation procedure can be traced for the understanding of the orderliness exhibited in other WFs in this study as well.

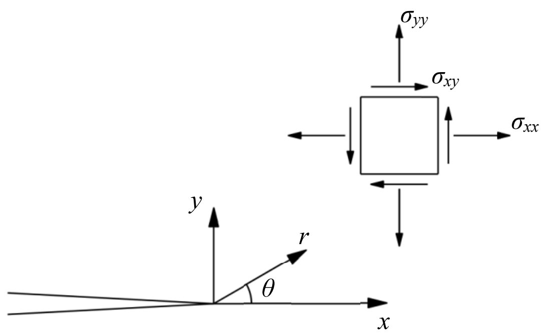


**Fig. 11.** Elastic stress field at crack-tip

As loads are generally applied on the top face of an RC beam, WFs on the top face are presented in this study as well. Referencing to **Fig. 5**, these WFs are given in a coordinate set-up that the point $E$ which is the closest point away from the crack tip on the top face is regarded as the origin and the direction from *F* to *D* is defined as the positive direction. Plots of $h_{Ix'}$, $h_{IIx'}$ and $h_{Iy'}$, $h_{IIy'}$ for loads along the top face for cracked geometries with the selected inclined angles are shown in **Fig. 12**. In $h_{Ix'}$ and $h_{IIx'}$, a continuous decreasing from maximum to almost zero in the region from *F* to *E* is observed, whereas $h_{Iy'}$ and $h_{IIy'}$ stay at a certain plateau in most of the same region and drop dramatically to almost zero just adjacent *E*. Due to an increasing content of local disturbing in the stresses around the crack tip as the applied load approaching the crack tip, a local fluctuation is observed in all curves within a small region adjacent to the point *E*. After the concerned point passes the disturbed region in the *F*-*D* direction, both $h_{Ix'}$, $h_{IIx'}$ and $h_{Iy'}$, $h_{IIy'}$ remain almost zero in the remaining region.

As a further step, the relation between WF and inclined angles should be deduced. Taking the $h_{Ix'}$ for example, firstly, for any given inclined angle, the distribution of $h_{Ix'}$ along the top face can be obtained by connecting the obtained corresponding nodal WFs for the VCE technique in FEM. The obtained distributions of the $h_{Ix'}$ for the selected 5 inclined angles are shown with solid curves in **Fig. 13(a)**. From **Fig. 12** and **13(a)**, it is found that for the points with a same distance away for the origin point *E* the $h_{Ix'}$ varies almost linearly with respect to the inclined angle. Thus, with the obtained distributions of $h_{Ix'}$ along the top face for any two inclined angles, e.g., 40° and 60°, the distribution of $h_{Ix'}$ for any other inclined angles among or outside of the range enclosed by the two angles may be obtainable employing either interpolation or extrapolation, respectively. Based on the linear interpolation, the $h_{Ix'}$ for the other three inclined angles are calculated and shown using isolated points in **Fig. 13(a)** together with the corresponding WF from VCE directly. It is found that the WFs from both approaches can match with each other very well. Actually, the discrepancy for any point in the whole region remains less than 1%.

As the other three WF components, i.e. $h_{IIx'}$, $h_{Iy'}$ and $h_{IIy'}$, exhibit a relation with the inclined angle similar to the $h_{Ix'}$ as shown in **Fig. 12**, one may be able to calculate the distributions of these three components for any inclined angles with the corresponding distributions of two inclined angles based on either the interpolation or extrapolation. Following the same procedure implemented on $h_{Ix'}$, the $h_{Iy'}$ of 3 inclined angles are obtained and shown in **Fig. 13(b)** with isolated points, where an excellent match is observed between the $h_{Iy'}$ from the VCE technique. Therefore, it may be concluded that if the WF components, i.e. $h_{Ix'}$ $h_{IIx'}$ and $h_{Iy'}$, $h_{IIy'}$, along the top face for two inclined angles are available, all the WFs for any other inclined angles can be by a linear interpolation or extrapolation of the corresponding WFs of the two available angles with a high accuracy.

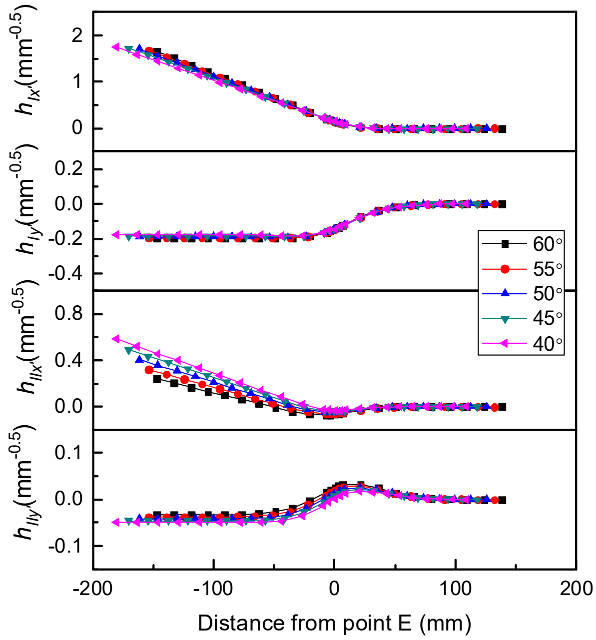


**Fig. 12.** Weight function variations with changing crack inclined angle for top face

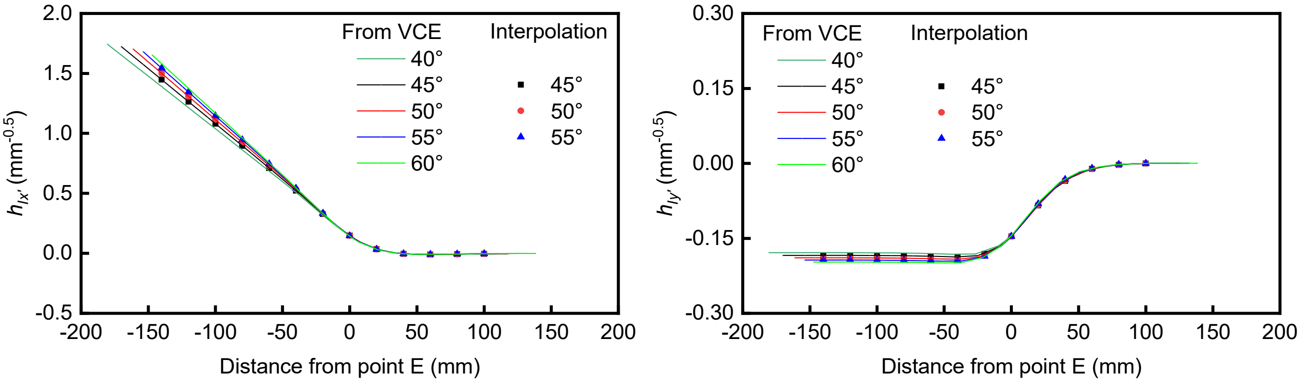


(a) Linear interpolation of $h_{Ix'}$ (b) Linear interpolation of $h_{Iy'}$

**Fig. 13.** Linear interpolation of $h_{Ix'}$ and $h_{Iy'}$ along the top face for different inclined angles

In an RC beam, any oblique shear crack is bridged by a series of stresses acting on the crack faces due to the existence of the concrete aggregates and reinforcement. Thus, a derivation of the relation between crack face WFs and the inclined angle are of great significances for calculating the crack tip SIFs as well as the COD profiles based on fracture mechanics. Considering that the stresses acting on crack faces are usually decomposed into bridging stress normal to crack faces and shearing stress tangent to crack faces, all of the crack face WF components named as $h_{Ix}$, $h_{IIx}$, $h_{Iy}$, and $h_{IIy}$ are given and investigated in the $(x, y)$ coordinate system as shown in **Fig. 5** to be more convenient to use. **Fig. 14** and **Fig. 15** show the distributions of $h_{Ix}$, $h_{IIx}$, $h_{Iy}$, and $h_{IIy}$ along the upper and lower crack faces for the inclined shear crack geometries with $\beta$=40°, 45°, 50°, 55° and 60°, where a $1/\sqrt{r}$ singular behavior of crack face WFs in crack tip neighborhood are observed in the primary WF components, i.e. $h_{IIx}$ and $h_{Iy}$. Since the absolute values of WFs for the upper and lower crack face show similar characteristics with respect to a variation of inclined, their relations with the inclined angle are analyzed together. Under the $(x, y)$ coordinate system, it is found that the WFs either stay almost unchanged or change almost linearly with respect to the inclined angle. Hence, similar to the WF components along the top face and left-hand face (see. **Fig. 5**), the distributions of crack face WFs for any inclined angles may be obtainable exploiting the corresponding WFs of two given inclined angles also based on the linear interpolation or extrapolation method. Taking the $h_{Ix}$ and $h_{Iy}$ (one secondary and one primary WF components) for example and using the $h_{Ix}$ and $h_{Iy}$ of inclined anlges 40° and 60° from VCE, the distributions of them for inclined angles 45°, 50°and 55° are calculated and shown together with the results from VCE directly in **Fig. 16**. It is found that the WFs from both approaches can match with each other very well. Actually, a less than 1% of error is achieved for any point in the whole investigated region. Therefore, it may be concluded that if the distributions of the WF components $h_{Ix}$, $h_{IIx}$, and $h_{Iy}$, $h_{IIy}$ along crack faces for two inclined angles are available, the WFs for any other inclined angles can be calculated accurately through interpolating or extrapolating the corresponding WFs for the two inclined angles.

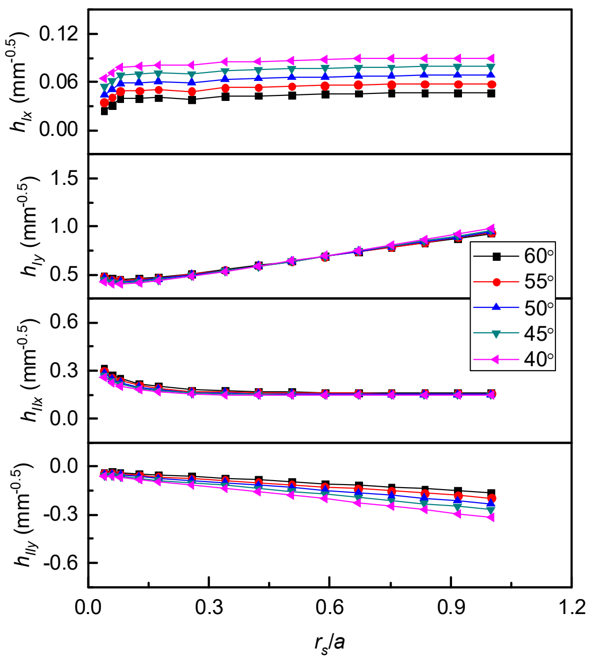


**Fig. 14.** Weight function variations with changing crack inclined angle for upper crack face

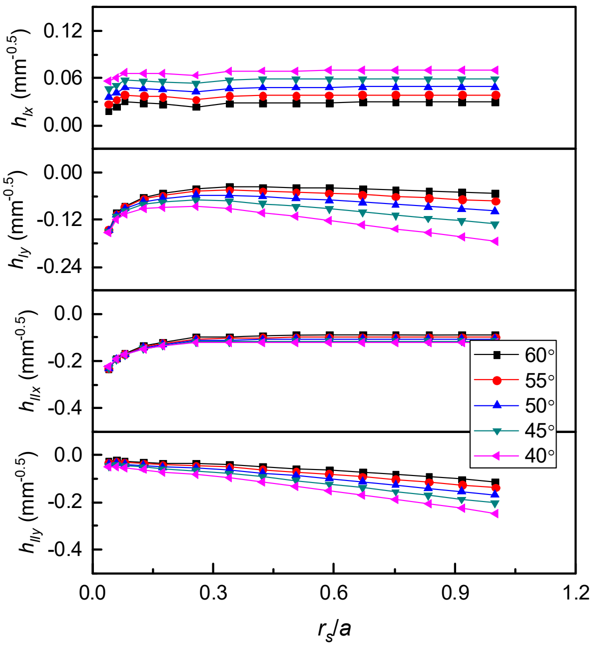


**Fig. 15.** Weight function variations with changing crack inclined angle for lower crack face

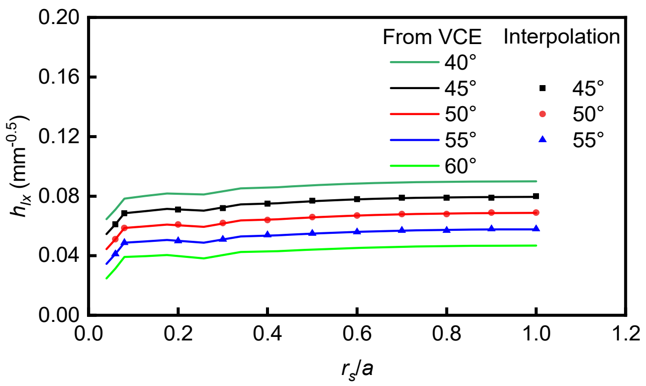


(a) Linear interpolation of $h_{Ix}$

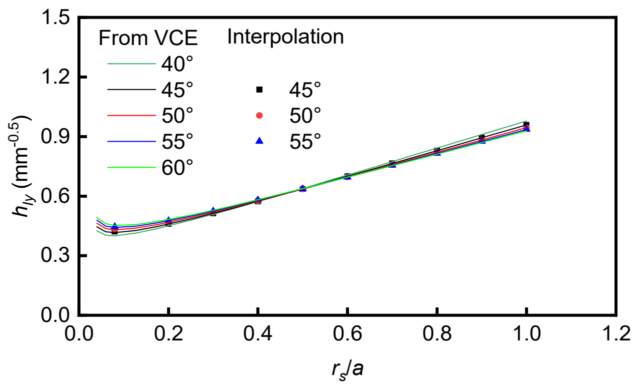


(b) Linear interpolation of $h_{Iy}$

**Fig. 16.** Linear interpolation of $h_{Ix}$ and $h_{Iy}$ along the upper crack face for different inclined angles

### 4.2.3 Weight function for varying crack initiation location

In this section, the relations between crack initiation location and WFs are investigated from analyzing the inclined cracked geometry (**Fig. 5**) with fixed geometrical dimensions ($h$=300mm and $w$=100mm), crack length

($a/w$=0.5), and inclined angle ($\beta$=45°), but varying crack initiation locations. As shown in **Fig. 4(b)**, the initiation location ($\varphi$) for most RC beams with different geometries and material properties ranges from 0.4 to 0.6. Therefore, the oblique edge crack geometries with inclined angles in this range are employed for the detailed WF calculation. With respect to the ($x'$, $y'$) coordinates, **Fig. 17** shows the WFs along the left-hand face for the inclined edge crack geometries with $\varphi$=0.4, 0.45, 0.5, 0.55 and 0.6 in relation to the distance away from the point $A$ in **Fig. 5**. It is found that for a given crack initiation location the WF components, $h_{Ix'}$ and $h_{IIx'}$, stay constant in the entire left-hand face, whereas the WF components, $h_{Iy'}$ and $h_{IIy'}$, vary linearly with respect to the distance away from the point $A$. In addition, the values of the constant $h_{Ix'}$ and $h_{IIx'}$ for the employed crack initiation locations are shown in **Fig. 18(a)** and **Fig. 18(b)**, respectively, where a linear relation is observed in both curves. In terms of the $h_{Iy'}$ and $h_{IIy'}$, almost no effect is observed due to a variation of the crack initiation location ($\varphi$). Actually, all these observed characteristics can be understood following **Eq. (16)** as well. Therefore, one may demonstrate that the WFs for shear cracked geometries with any crack initiation locations can be calculated accurately through interpolating or extrapolating the corresponding WFs for the two crack initiation locations.

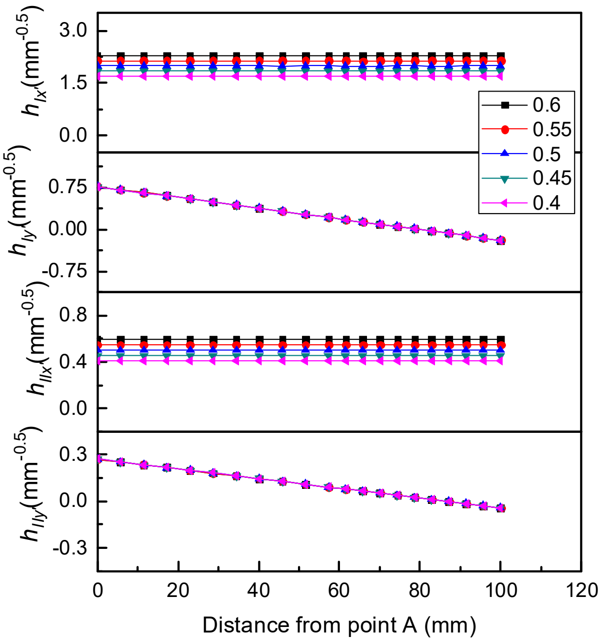


**Fig. 17.** Weight function variations with changing crack initiate location for left-hand face

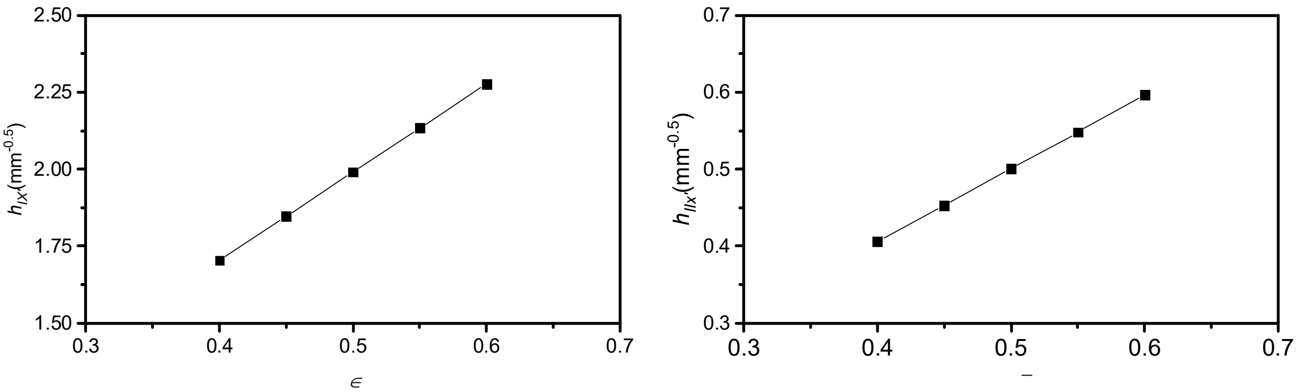


(*a*) $h_{Ix'}$ (*b*) $h_{IIx'}$

**Fig. 18.** Constant values of $h_{Ix'}$ and $h_{IIx'}$ with respect to distance from Point A on left-hand face for different crack initiate locations

With respect to the ($x'$, $y'$) coordinate system and the ($x$, $y$) coordinate system, the WF components along the top face and the crack faces including the upper and lower ones are shown in **Fig. 19**, **Fig. 20**, and **Fig. 21**, respectively. As the WF distributions along the top face are given with respect to the point $E$ which is the closest point from the crack tip as shown in **Fig. 5**, no observable change due to a variation of the crack initiation location is exhibited in **Fig. 19**. In terms of the crack faces, due to the fixed inclined angle and crack length, except for the $h_{Ix}$ on both upper and lower crack faces, all the other WF components remain almost unchanged with respect to the variation of the crack initiation location as shown in **Fig. 20** and **Fig. 21**. Even for $h_{Ix}$ on both upper and lower crack faces, their variations are pretty small in the selected wide range for $\varphi$, i.e. from 0.4 to 0.6. Besides, as the $h_{Ix}$ is the secondary WF component for the Mode I fracture, the absolute values of it are much smaller than the absolute values of the corresponding primary WF component for the Mode I fracture, i.e. $h_{Iy}$. This means that, for applications, these minor influences of crack initiation location on $h_{Ix}$ may be negligible. Therefore, for the inclined crack geometries with any $\varphi$, the WF components along the top face, upper and lower crack faces for the geometry with a given $\varphi$ can be exploited without any modification.

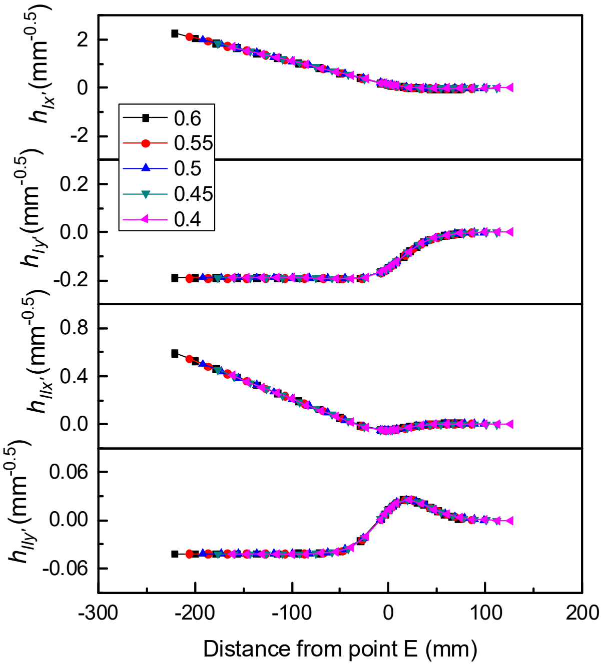


**Fig. 19.** Weight function variations with changing crack initiate location for top face

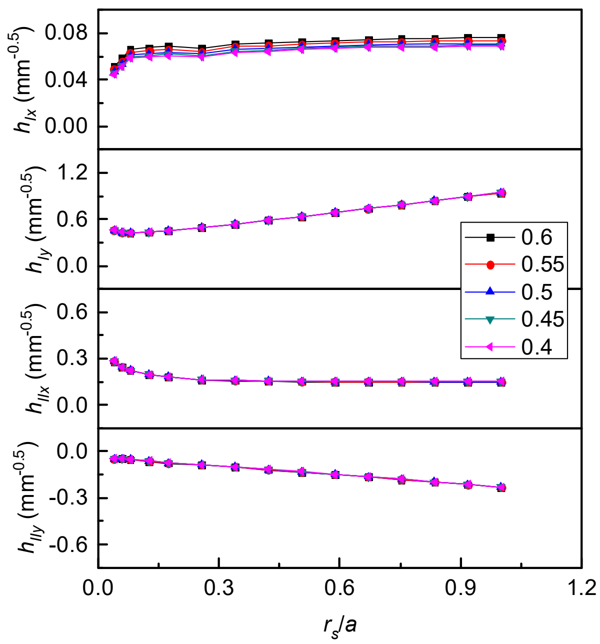


**Fig. 20.** Weight function variations with changing crack initiate locations for upper crack face

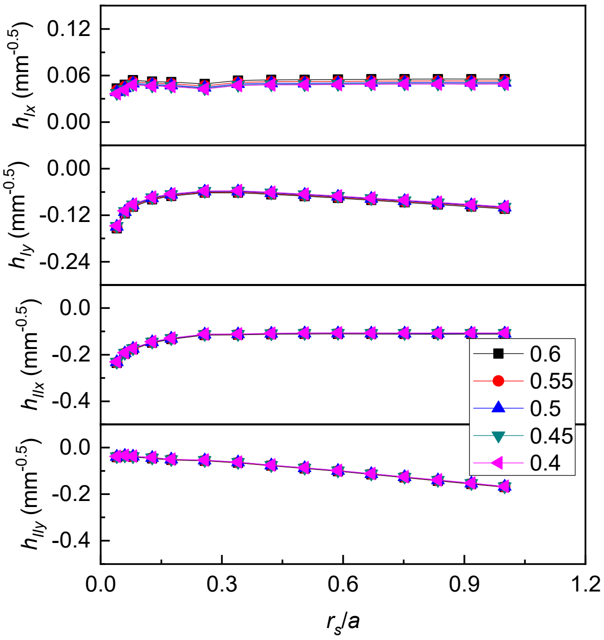


**Fig. 21.** Weight function variations with changing crack initiate locations for lower crack face

#### 4.2.4 Weight function for varying shear span to beam depth ratio

The relations between the shear span to beam depth ratio ($\omega$) and WFs are investigated and summarized in this section by fixing the beam depth ($w$=100mm), crack length ($a/w$=0.5), inclined angle ($\beta$=45°), and crack initiation location ($\varphi$ =0.6). As it was reported that a critical shear which leads to the failure of an RC beam occurs only in a beam with a shear span to beam depth ratio range from 2.0 to 8.0 [27, 38]. Thus, this study employs three shear span/beam depth ratios, i.e. 2.5, 5.0 and 7.5, which is considered to be wide enough.

With respect to the ($x'$, $y'$) coordinates, **Fig. 22** shows the WFs along the left-hand face for the inclined crack geometries with $\omega$=2.5, 5.0, and 7.5 in relation to the distance away from the point $A$ in **Fig. 5**. Similar to the previous sections, a constant $h_{Ix'}$ and $h_{IIx'}$ and a linearly varying $h_{Iy'}$ and $h_{IIy'}$ are observed for each shear span/beam depth ratio. Moreover, the constant values of $h_{Ix'}$ and $h_{IIx'}$ to $\omega$ relations are provided in **Fig. 23**, where a linear correlation is exhibited. Thus, in terms of the WF components of the left-hand face, it may be stated that one can obtain them of any shear span/beam depth ratios with high accuracy based on interpolation or extrapolation method if they are available for two different shear span/beam depth ratios.

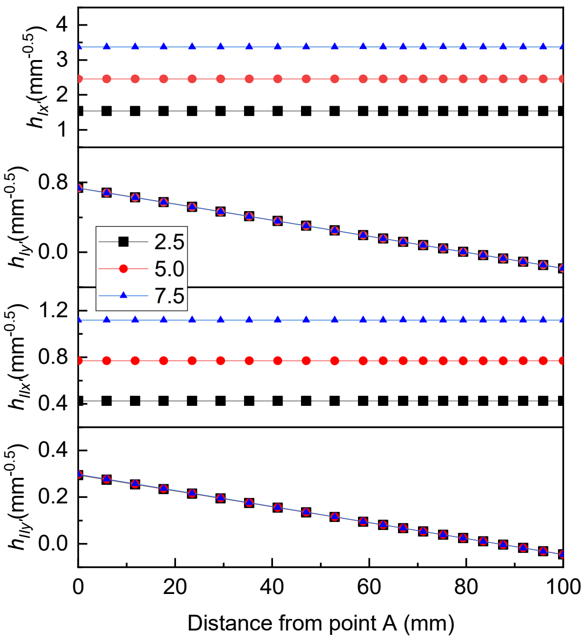


**Fig. 22.** Weight function variations with changing shear span ratios for the left-hand face

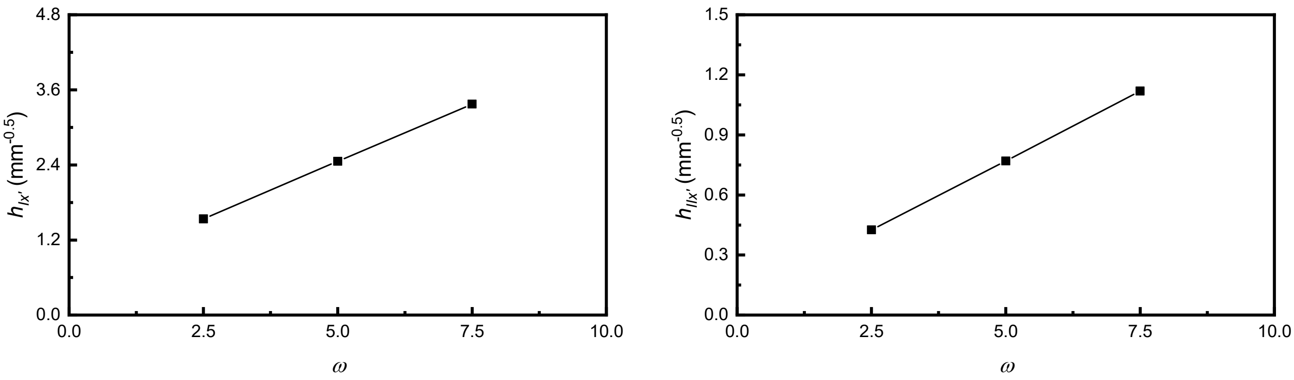


(*a*) $h_{Ix'}$ (*b*) $h_{IIx'}$

**Fig. 23.** Constant values of $h_{Ix'}$ and $h_{IIx'}$ with respect to distance from Point A on left-hand face for different shear span ratios

With respect to the ($x'$, $y'$) and ($x$, $y$) coordinate systems, the distributions of WFs along the top face and crack faces (see. **Fig. 5**) are shown in **Fig. 24** as well as **Fig. 25-26**, respectively, for the employed shear span/beam depth ratios. In terms of the WFs along the top face, it is found that the WF distribution of one larger value of $\omega$ behaves like an extension of corresponding WF distribution of another $\omega$ with a smaller value along both directions away from the point $E$ (see. **Fig. 5**). As for WF distributions along the upper and lower crack faces as shown in **Fig. 25** and **Fig. 26**, almost no difference is observed among the employed shear span/beam depth ratios. Therefore, if a set of WF distributions of these three components is available for one shear span/beam depth ratio, the WF distributions for the inclined cracked geometries with any $\omega$ can be easily calculated.

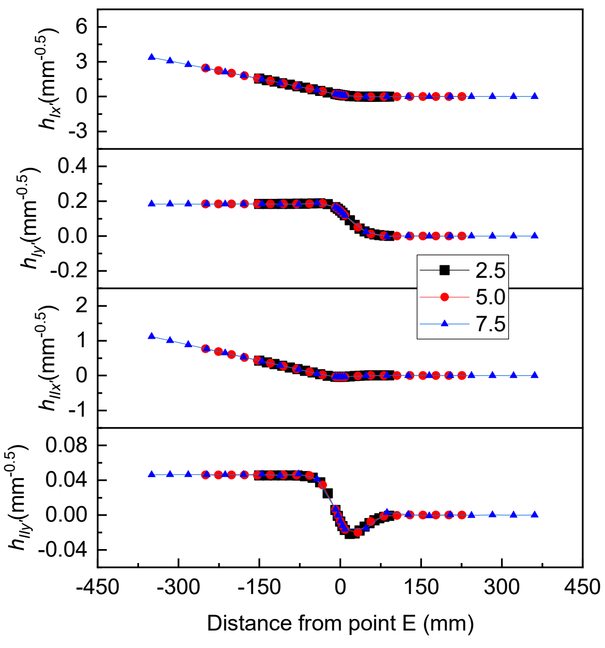


**Fig. 24.** Weight function variations with changing shear span ratios for top face

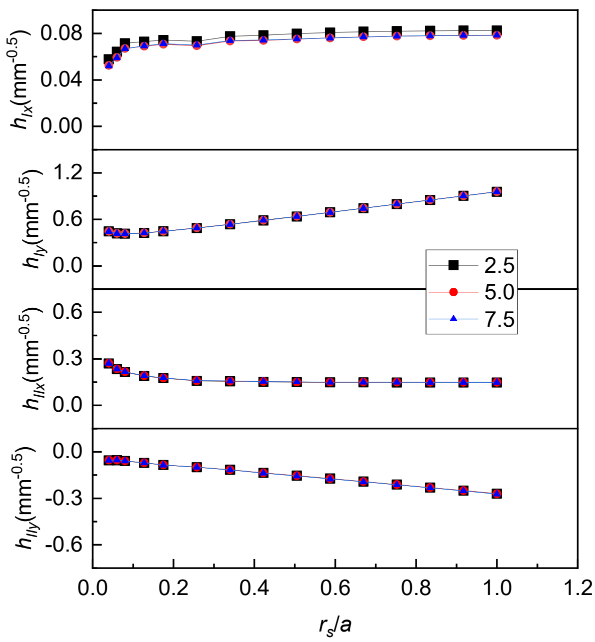


**Fig. 25.** Weight function variations with changing shear span ratios for upper crack face

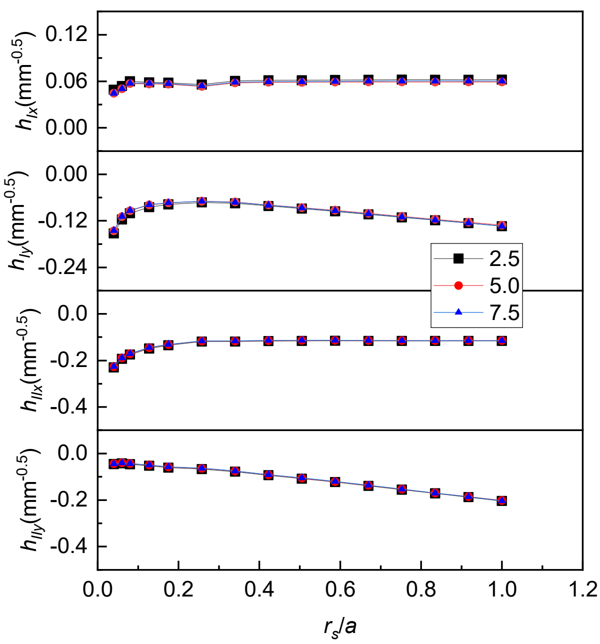


**Fig. 26.** Weight function variations with changing shear span ratios for lower crack face

## 5 WEIGHT FUNCTIONS FOR SHEAR CRACKS WITH ANY GEOMETRY

### 5.1 Summary of the relation between weight functions and geometrical properties

According the obtained relations between the geometrical properties which determine a shear cracked beam and the WFs along the boundaries generally subjected to loads in the previous sections, it is found that, due to a variation of one geometrical property, the WFs along all the boundaries can be easily calculated if the corresponding WFs of cracked geometries with one or two different values of the varying property are given. To facilitate application, **Table 1** summaries the number of cases where the cracked geometries have one different property and the WFs should be available to obtain the WFs of geometries with any values of the property. Besides, the corresponding calculation method is provided in **Table 1** as well.

**Table 1** Summary of number of cases should be given for all possible geometric variations, general load applied boundaries and WFs

<table>
<tr><th rowspan="2">Geometric variation</th><th rowspan="2">Boundaries</th><th colspan="4">No. of cases should be given</th></tr>
<tr><th>$h_{Ix}$ or $h_{Ix'}$</th><th>$h_{IIx}$ or $h_{IIx'}$</th><th>$h_{Iy}$ or $h_{Iy'}$</th><th>$h_{IIy}$ or $h_{IIy'}$</th></tr>
<tr><td rowspan="4">Absolute size</td><td>Left-hand face</td><td colspan="4" rowspan="4">One case<br>Multiplying $1/\sqrt{n}$<br>($n$ is multiples for absolute size)</td></tr>
<tr><td>Top face</td></tr>
<tr><td>Upper crack face</td></tr>
<tr><td>Lower crack face</td></tr>
<tr><td rowspan="4">Inclined angle ($\beta$)</td><td>Left-hand face</td><td colspan="4" rowspan="4">Two cases<br>Linear interpolation or extrapolation</td></tr>
<tr><td>Top face</td></tr>
<tr><td>Upper crack face</td></tr>
<tr><td>Lower crack face</td></tr>
<tr><td rowspan="4">Crack initiate location ($\varphi$)</td><td>Left-hand face</td><td colspan="2" rowspan="2">Two cases<br>Linear interpolation or extrapolation</td><td colspan="2" rowspan="2">One case<br>Exploit directly</td></tr>
<tr><td>Top face</td></tr>
<tr><td>Upper crack face</td><td colspan="4" rowspan="2">One case<br>Exploit directly</td></tr>
<tr><td>Lower crack face</td></tr>
<tr><td rowspan="4">Shear span/beam depth ($\omega$)</td><td>Left-hand face</td><td colspan="2">Two cases<br>Linear interpolation or extrapolation</td><td colspan="2">One case<br>Exploit directly</td></tr>
<tr><td>Top face</td><td colspan="4">One case<br>Extension or clip</td></tr>
<tr><td>Upper crack face</td><td colspan="4" rowspan="2">One case<br>Exploit directly</td></tr>
<tr><td>Lower crack face</td></tr>
</table>

### 5.2 Method of calculating weight function with any geometry

From **Table 1**, it is found that, in terms of the variation of one geometrical property except for the absolute size, the WFs for any values of the property can be obtained by either exploiting a given set of WFs or linearly interpolating/extrapolating two given sets of WFs. To be unified, the linear interpolation or extrapolation method may be used for every property and all WF components. As a result, one can calculate the WFs of a shear cracked beam with an arbitrary geometry, where the beam depth, shear span, inclined angle, crack initiate location (see. **Fig. 5**) are assumed and named as $w^a$, $\omega^a$, $\beta^a$, $\varphi^a$ with a superscript "$a$" indicating "arbitrary", as follows. Step 1: calculating the WFs of any shear cracked geometries with varying $\omega$, $\beta$ and $\varphi$, but fixed absolute size, in other words, fixed beam depth ($w$=100 mm). For a beam with a 100 mm of beam depth, the linear relation between the WFs and the geometrical properties can be expressed mathematically as

$$\frac{\partial WF(100,\omega,\beta,\varphi)}{\partial(\omega)}=\mu_1 \tag{17a}$$

$$\frac{\partial WF(100,\omega,\beta,\varphi)}{\partial(\beta)}=\mu_2 \tag{17b}$$

$$\frac{\partial WF(100,\omega,\beta,\varphi)}{\partial(\varphi)}=\mu_3 \tag{17c}$$

where $WF(100,\omega,\beta,\varphi)$ is the weight function of the beam depth equaling 100 mm. $\mu_1$, $\mu_2$, and $\mu_3$ are constants and also the slope of the relations between the WFs to the shear span/beam depth ratio, inclined angle, and crack initiation location. Through solving the partial derivative equations (**Eq. (17)**), one can obtain the $WF(100,\omega,\beta,\varphi)$ as follows

$$WF(100,\omega,\beta,\varphi)=\mu_1\cdot\omega+\mu_2\cdot\beta+\mu_3\cdot\varphi+C \tag{18}$$

where $C$ is a constant, which may be determined if the WF for one set of $\omega$, $\beta$, and $\varphi$ is available. In fact, any shear cracked geometry among the calculated ones in this study can be the set, and the corresponding WF can be employed. Besides, a linear combination is used in **Eq. (18)** because the equation is derived from solving the partial differential equation and the weight function is a concept in the scope of linear elastic fracture mechanics. As the WF acts as a reference, it is named as $WF(100, \omega^r, \beta^r, \varphi^r)$. Substituting it into **Eq. (18)**, one can obtain the constant $C$, and the **Eq. (18)** is transferred into the following one

$$WF(100, \omega, \beta, \varphi) = \mu_1 \cdot (\omega - \omega^r)\omega + \mu_2 \cdot (\beta - \beta^r) + \mu_3 \cdot (\varphi - \varphi^r) + WF(100, \omega^r, \beta^r, \varphi^r) \tag{19}$$

where $\omega^r$, $\beta^r$, and $\varphi^r$ are the geometrical properties of the reference case.

In terms of the $\mu_1$, $\mu_2$, and $\mu_3$, they can be calculated using the WFs of any two different shear span/beam depth ratio, inclined angles, and crack initiation locations, respectively, as follows

$$\mu_1 = \frac{WF(100, \omega_1, \beta, \varphi) - WF(100, \omega_2, \beta, \varphi)}{\omega_1 - \omega_2} \tag{20a}$$

$$\mu_2 = \frac{WF(100, \omega, \beta_1, \varphi) - WF(100, \omega, \beta_2, \varphi)}{\beta_1 - \beta_2} \tag{20b}$$

$$\mu_3 = \frac{WF(100, \omega, \beta, \varphi_1) - WF(100, \omega, \beta, \varphi_2)}{\varphi_1 - \varphi_2} \tag{20c}$$

where $WF(100, \omega_1, \beta, \varphi)$ and $WF(100, \omega_2, \beta, \varphi)$ are the WFs for two different shear span/beam depth ratios, $\omega_1$ and $\omega_2$, respectively. $WF(100, \omega, \beta_1, \varphi)$ and $WF(100, \omega, \beta_2, \varphi)$ are the WFs for two different inclined angles, $\beta_1$ and $\beta_2$, respectively. $WF(100, \omega, \beta, \varphi_1)$ and $WF(100, \omega, \beta, \varphi_2)$ are the WFs for two different crack initiation locations, $\varphi_1$ and $\varphi_2$, respectively. All these WFs are calculated and provided in the **section 4**.

Step 2: calculate the WFs for any shear cracked geometries. Based on a theoretical deviation in the **section 4.2.1**, a relation between the WFs and the absolute size is obtained and given in **Table 1**. As the absolute size of two geometries which have the same $\omega$, $\beta$, and $\varphi$ can be represented by the absolute value of any one dimension including the beam depth ($w$=100 mm), the WFs of the aimed cracked beam with an arbitrary geometry ($WF(w, \omega, \beta, \varphi)$) can be calculated using the $WF(100, \omega, \beta, \varphi)$ from Step 1 as:

$$WF(w, \omega, \beta, \varphi) = \frac{WF(100, \omega, \beta, \varphi)}{\sqrt{w/100}} \tag{21}$$

and then substituting the values of $w^a$ $\omega^a$, $\beta^a$, $\varphi^a$ into **Eq. (21)**.

## 6 CONCLUSIONS

This paper proposes a WF calculating method for shear cracked RC beams with any geometrical properties through investigating the laws inherently contained in the corresponding nodal WFs obtained from a VCE technique in FEM. The proposed method makes the fracture mechanics based analytical studies on shearing behaviors and strength of RC beams possible. The main conclusions are:

(1) As a critical shear crack determines the behavior of shear critical RC beams, the critical shear crack geometries for a large set of RC beams were predicted. It was found that the crack inclined angle and crack initiation location for most RC beams fall in ranges {40°, 60°} and {0.4, 0.6}, respectively.

(2) The variations of WFs for shear cracked RC beams with respect to any geometrical property, which determines the beams including the absolute size, crack inclined angle, crack initiation location and shear span/beam depth ratio, can be evaluated accurately using the corresponding WFs of crack geometries with only one or two different values of this property based on a linear interpolating/extrapolation method.

(3) Exploiting the WFs provided in this study and following a linear interpolating/extrapolation method, an equation of calculating the WFs for shear cracked RC beams with any geometrical properties was derived for all of boundaries generally subjected to external loads. Due to the relatively simple format of the equation, it may be stated that the developed method is friendly to engineering applications.

(4) As the WF has a load independent characteristic, the applications of the proposed WF calculation method may be extended to shear cracked beams made of other materials, such as FRC and ECC, or reinforced with other members, such as FRP tendons, if the nonlinearities contained in the crack bridging elements can be represented by a bridging stress to crack width relation separately.

## DECLARATION OF COMPETING INTEREST

The authors would like to declare that they no competing financial, professional, or personal interests from other parties.

## REFERENCES


[1] Vecchio F, Collins M. Investigating the collapse of a warehouse. ACI Concrete International; 1990, 12(3), 72-78.

[2] ACI B. 318-Building code requirements for reinforced concrete and commentary. American Concrete Institute International; 1999.

[3] Eurocode 2. Design of Concrete Structures: Part 1: General Rules and Rules for Buildings. European Committee for Standardization; 1991.

[4] Collins MP, Bentz EC, Sherwood EG. Where is shear reinforcement required? Review of research results and design procedures. ACI Structural Journal; 2008, 105(5), 590.

[5] Taylor HPJ. Investigation of the forces carried across cracks in reinforced concrete beams in shear by interlock of aggregate (No. TR 42.447 Tech. Rpt); 1970.

[6] Sherwood EG, Bentz EC, Collins MP. Effect of aggregate size on beam-shear strength of thick slabs. ACI Structural Journal; 2007, 104(2), 180.

[7] Fenwick R, Pauley T. Mechanism of shear resistance of concrete beams. Journal of the Structural Division; 1968, 94(10), 2325-2350.

[8] Walraven JC. Fundamental analysis of aggregate interlock. Journal of the Structural Division; 1981, 107(11), 2245-2270.

[9] Bueckner HF. Field singularities and related integral representations methods of analysis and solutions of crack problems (pp. 239-314): Springer; 1973.

[10] Rice JR. Some remarks on elastic crack-tip stress fields. International Journal of Solids and Structures; 1972, 8(6), 751-758.

[11] Reinhardt HW, Cornelissen HA, Hordijk DA. Tensile tests and failure analysis of concrete. Journal of Structural Engineering; 1986, 112(11), 2462-2477.

[12] Tada H, Paris P, Irwin G. The analysis of cracks handbook. New York: ASME Press, 2, 1; 2000.

[13] Nazmul I, Matsumoto T. High resolution COD image analysis for health monitoring of reinforced concrete structures through inverse analysis. International Journal of Solids and Structures; 2008a, 45(1), 159-174.

[14] Nazmul I, Matsumoto T. Regularization of inverse problems in reinforced concrete fracture. Journal of Engineering Mechanics; 2008b, 134(10), 811-819.

[15] Deng P, Matsumoto T. Estimation of the rebar force in RC members from the analysis of the crack mouth opening displacement based on fracture mechanics. Journal of Advanced Concrete Technology; 2017a, 15(2), 81-93.

[16] Matsumoto T, Li VC. Fatigue life analysis of fiber reinforced concrete with a fracture mechanics based model. Cement and Concrete Composites; 1999, 21(4), 249-261.

[17] Zhang J, Stang H, Li VC. Crack bridging model for fibre reinforced concrete under fatigue tension. International Journal of Fatigue; 2001, 23(8), 655-670.

[18] Suthiwarapirak P, Matsumoto T. Fatigue analysis of RC slabs and repaired RC slabs based on crack bridging degradation concept. Journal of Structural Engineering; 2006 132(6), 939-948.

[19] Wang B, Wang Z, Uji K, Zhang J, Guo R. Experimental investigation on shear behavior of RC beams strengthened by CFRP grids and PCM. Structures; 2020, 27, 1994-2010.

[20] George TS. Stiffness derivative finite element technique to determine nodal weight functions with singularity elements. Engineering Fracture Mechanics; 1984, 19(4), 685-699.

[21] George TS, Chien-Tung Y. Weight function calculations for mixed mode fracture problems with the virtual crack extension technique. Engineering Fracture Mechanics; 1985, 21(6), 1119-1149.

[22] Deng P, Matsumoto T. Weight function determinations for shear cracks in reinforced concrete beams based on finite element method. Engineering Fracture Mechanics; 2017b, 177, 61-78.

[23] Deng P, Matsumoto T. Determination of dominant degradation mechanisms of RC bridge deck slabs under cyclic moving loads. International Journal of Fatigue; 2018, 112, 328-340.

[24] Deng P, Matsumoto T. Fracture Mechanics–Based Fatigue Life Prediction Method for RC Slabs in Punching Shear Failure Mode. Journal of Structural Engineering; 2020, 146(1), 04019186.

[25] Ahmad S, Bhargava P.. Shear strength models for reinforced concrete slender beams: a comparative study. Structures; 2018, 16, 119-128.

[26] Tahenni T, Bouziadi F, Boulekbache B, Amzian S. Experimental and nonlinear finite element analysis of shear behaviour of reinforced concrete beams. Structures; 2021, 29, 1582-1596.

[27] Zararis PD, Papadakis GC. Diagonal shear failure and size effect in RC beams without web reinforcement. Journal of Structural Sngineering; 2001, 127(7), 733-742.

[28] Ishikawa H, Kitagawa H, Okamura H. J integral of a mixed mode crack and its application. Mechanical Behaviour of Materials; 1980, 447-455.

[29] Walraven JC. Fundamental analysis of aggregate interlock. Journal of the Structural Division; 1981, 107(11), 2245-2270.

[30] Papadakis G. Shear failure of reinforced concrete beams without stirrups. PhD diss., Department of Civil Engineering; 1996, Aristotle University of Thessaloniki, Thessaloniki, Greece (in Greek).

[31] Mphonde AG, Frantz GC. Shear tests of high-and low-strength concrete beams without stirrups. Paper presented at the Journal Proceedings; 1984, 81(4), 350-357.

[32] Leonhardt F, Walther R. Shear tests on beams with and without shear reinforcement. Deutscher Ausschuss für Stahlbeton; 1962, (151), 83.

[33] Collins MP, Kuchma D. How safe are our large, lightly reinforced concrete beams, slabs, and footings? Structural Journal; 1999, 96(4), 482-490.

[34] Chana P. Some aspects of modelling the behaviour of reinforced concrete under shear loading, No. Monograph; 1981.

[35] Bhal N. On the influence of beam depth on shear capacity of single-span RC beams with and without shear reinforcement. PhD dissertation, Universität Stuttgart, Stuttgart, Germany; 1968.

[36] Altoubat S, Yazdanbakhsh A, Rieder KA. Shear behavior of macro-synthetic fiber-reinforced concrete beams without stirrups. ACI Materials Journal; 2009, 106(4).

[37] Ingraffea AR, Manu C. Stress-intensity factor computation in three dimensions with quarter-point elements. International Journal for Numerical Methods in Engineering; 1980, 15(10), 1427-1445.

[38] Muttoni A, Fernández Ruiz M. Shear strength of members without transverse reinforcement as function of critical shear crack width. ACI Structural Journal; 2008, 105, 163-172.